ISPRS Journal of Photogrammetry and Remote Sensing 103 (2015) 81–92

Contents lists available at ScienceDirect

ISPRS Journal of Photogrammetry and Remote Sensing

journal homepage: www.elsevier.com/locate/isprsjprs

Use of Landsat and Corona data for mapping forest cover change from the mid-1960s to 2000s: Case studies from the Eastern United States and Central Brazil

Dan-Xia Song *, Chengquan Huang, Joseph O. Sexton, Saurabh Channan, Min Feng, John R. Townshend

Global Land Cover Facility, Department of Geographical Sciences, University of Maryland, College Park, MD 20742, USA

ARTICLE INFO

Article history:
Received 30 June 2013
Received in revised form 9 February 2014
Accepted 11 September 2014
Available online 5 October 2014

Keywords:
Corona
Landsat
Forest cover
Change detection
Image texture

ABSTRACT

Land-cover change detection using satellite remote sensing is largely confined to the era of Landsat satellites, from 1972 to present. However, the Corona, Argon, and Lanyard intelligence satellites operated by the U.S. government between 1960 and 1972 have the potential to provide an important extension of the long-term record of Earth's land surface. Recently declassified, the archive of images recorded by these satellites contains hundreds of thousands of photographs, many of which have very high ground resolution- 6–9 ft (1.8–2.7 m) even by today's standards. This paper demonstrates methods for extending the span of forest-cover change analysis from the Landsat-5 and -7 era (1984 to present) to the previous era covered by the Corona archive in two study areas: one area covered predominantly by urban and sub-urban land uses in the eastern US and another area by tropical forest in central Brazil. We describe co-registration of Corona and Landsat images, extraction of texture features from Corona images, classification of Corona and Landsat images, and post-classification change detection based on the resulting thematic dataset. Second-order polynomial transformation of Corona images yielded geometric accuracy relative to Landsat-7 of 18.24 m for the urban area and 29.35 m for the tropical forest study area, generally deemed adequate for pixel-based change detection at Landsat resolution. Classification accuracies were approximately 95% and 96% for forest/non-forest discrimination for the temperate urban and tropical forest study areas, respectively. Texture within 7 × 7- to 9 × 9-pixel (~13.0–16.5 m) neighborhoods and within 11 × 11-pixel (~30 m) neighborhoods were the most informative metrics for forest classification in Corona images in the temperate and tropical study areas, respectively. The trajectory of change from the 1960s to 2000s differed between the two study areas: the average annual forest loss rate in the urban area doubled from 0.68% to 1.9% from the 1960s to the mid-1980s and then decreased during the following decade. In contrast, deforestation in the Brazilian study area continued at a slightly increased pace between the 1960s and 1990s at annual loss rate of 0.62–0.79% and quickly slowed down afterward. This study demonstrates the strong potential of declassified Corona images for detecting historical forest changes in these study regions and suggests increased utility for retrieving a wide range of land cover histories around the world.

1. Introduction

The launch of the first Landsat satellite (named the "Earth Resource Technology Satellite", ERTS-1) in 1972 opened an era of monitoring Earth's terrestrial surface by space-borne, remotely sensed imagery. Over the following decades, the medium spatial resolution, global coverage, and potential for time-serial analysis of the Landsat data record have enabled assessments of forest[1] change from local to national scales (Brandt et al., 2012; Huang et al., 2009; Sexton et al., 2013). Recently, global Landsat datasets have facilitated forest change analysis at the global scale (Townshend et al., 2012).

[1] The definition of forest in this study follows the International Geosphere-Biosphere Programme (IGBP) definition of greater than or equal to 30% tree cover and height exceeding 2 m. Forest loss is defined as conversion from forest to other land cover. Forest gain is defined as growth or recovery of tree cover, such that a previous non-forest location subsequently meets the tree-cover criteria for forests.

* Corresponding author.

http://dx.doi.org/10.1016/j.isprsjprs.2014.09.005

However, in many parts of the world, large-scale forest changes occurred prior to the Landsat era. For example, eastern Paraguay was once covered by intact forests, but only 73.4 ± 4.9% of the original Atlantic forest was left by the 1970s (Huang et al., 2009; Nagel, 1991; Nickson, 1981). In southern Brazil, agricultural developments in the 1960s and 1970s resulted in the consolidation of small farms and a shift from labor-intensive crops to extensive ranching and soy production (Richards, 2011), which resulted in a large forest area being cleared. Knowledge of land cover prior to the Landsat era is important for fully understanding the impact of socioeconomic activities on natural resources, especially in regions where significant development had occurred before the 1970s.

Images acquired by the U.S. Key Hole (KH) missions, which consisted of the Corona, Argon, and Lanyard satellites (collectively referred to as "Corona" images hereafter) that operated from 1960 to 1972 (McDonald, 1995), have the potential to extend historical land cover mapping from the Landsat era into the 1960s. KH-4, including 4A and 4B, was the most successful mission series that acquired most of fine images during from early 1960s to early 1970s. Declassified Corona imagery has worldwide spatial coverage, especially in Eastern Europe and Asia (Fig. 1), and has very high ground resolutions, ranging from 6 to 9 feet (about 1.83–2.74 m). Declassified satellite images have been used to study boreal forest decline (Rigina, 2003), vegetation dynamics (Kadmon and Harari-Kremer, 1999), land resource change (Tappan et al., 2000), forest fire carbon emissions (Isaev et al., 2002), ice sheet change (Bindschadler and Vornberger, 1998), and archaeological features (Beck et al., 2007; Casana and Cothren, 2008; Challis et al., 2002). In these localized studies, Corona images were analyzed mainly through visual interpretation and manually tuned histogram segmentation or were used as stereo image pairs for extracting digital elevation models (DEMs). Although the spatial coverage of available Corona data may allow large-area applications for many parts of the world, such applications would be possible only using more automated digital image analysis methods.

The purpose of this study is to develop an approach for extending forest change monitoring back to the 1960s using Corona data. Focusing on increasing automation relative to earlier approaches, major methodological components of this approach include georegistration between Corona and Landsat images, extraction of texture features from Corona images, classification of Corona and Landsat images, and change detection based on the classification results. The effectiveness of this approach is demonstrated by mapping forest cover change between four epochs—1960s, 1980s, 1990s, and 2000s—in two study areas that have experienced major anthropogenic forest changes: an urbanized landscape in the eastern United States and a forested area in central Brazil characterized by recent agricultural expansion. The following sections provide a brief description of the study areas and datasets, followed by a detailed description of the various methodological components and results derived using these methods. The paper closes with a discussion of potential improvements and applications of the approach developed in this study.

2. Study area and data

2.1. Study area

Two study areas with widely different vegetation properties and human land uses were selected to determine the feasibility of using paired Corona and Landsat images for detecting forest changes (Fig. 2). The sites were selected to represent the range of forest types and change trajectories that impact forest cover classification of high resolution remote sensing images and change detection. The Virginia-Maryland (VM) study area in the eastern United States, centered at 39°02′34.63″N, 77°23′35.45″W and spanning 32.6-by-23.6 km, lies within the temperate mixed forest biome and experienced forest change due to urbanization and managed forest planting. Forests in this region comprise a mix of deciduous (e.g. oak and hickory) and evergreen (e.g. loblolly pine) species. The leaf-on season for deciduous forest normally starts in early April and ends in

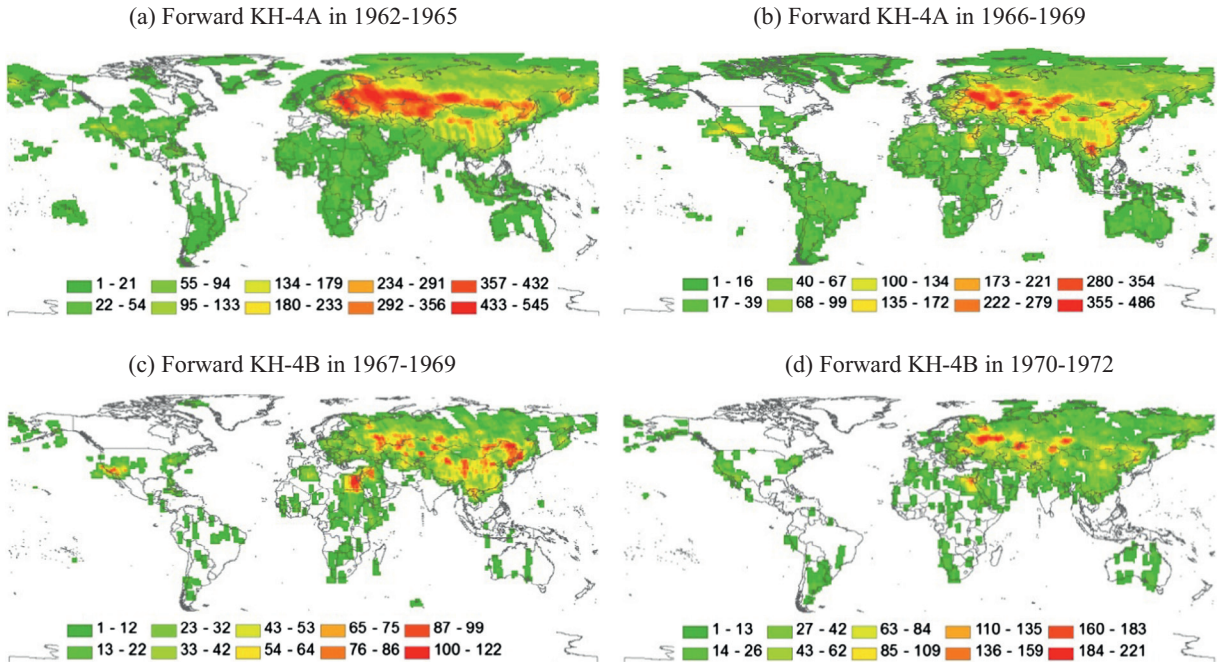

Fig. 1. Global coverage of Corona images acquired by the forward-looking cameras during the KH-4A and KH-4B missions. All coverage maps have been rasterized for display purposes from vector format to 1° geographic grid. (a) KH-4A mission between 1962 and 1965; (b) KH-4A mission between 1966 and 1969; (c) KH-4B mission between 1967 and 1969; and (d) KH-4B mission between 1970 and 1972 (*Source:* https://lta.cr.usgs.gov/declass_1). Metadata was downloaded from U.S. Geological Survey (USGS) Earth Explorer website.

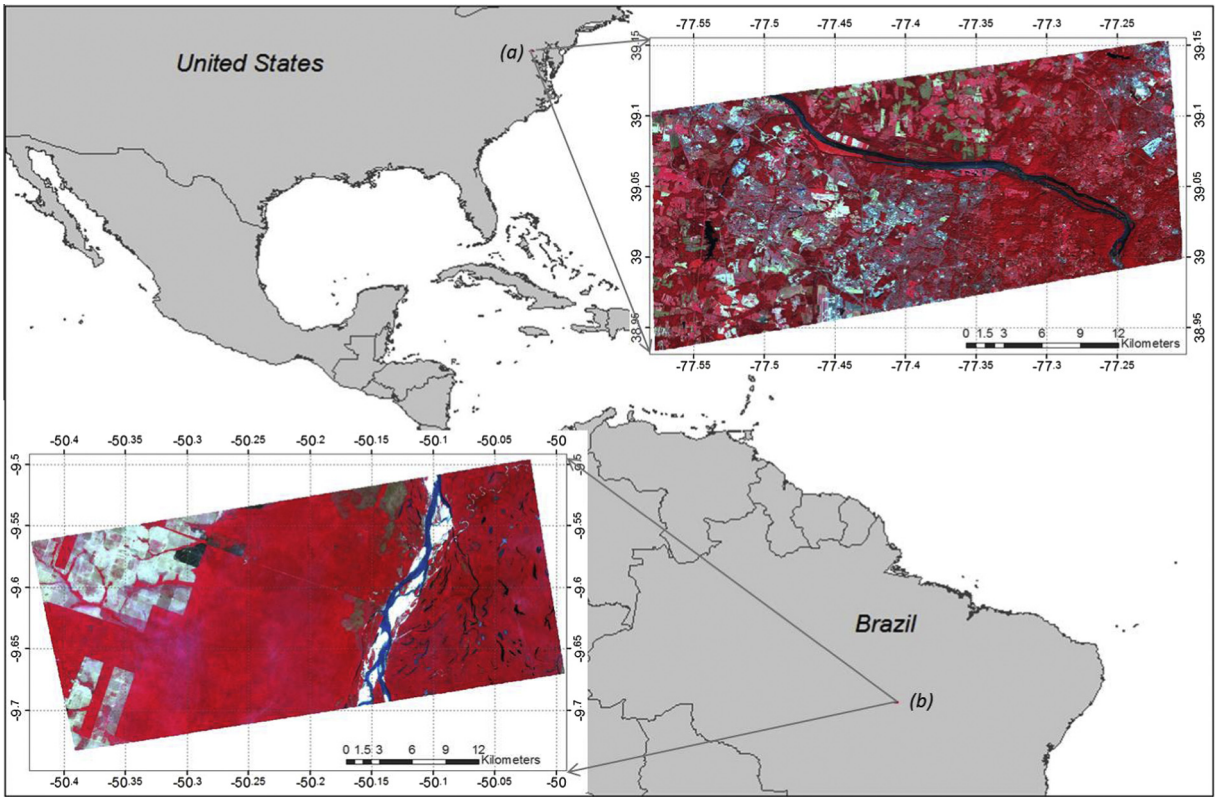

Fig. 2. Location of the Virginia–Maryland (VM) study area in eastern US (top) and the Mato Grosso-Tocantins-Pará (MTP) study area in central Brazil (bottom), and the zoomed GLS 2000 images for the two study areas shown with band 4 3 2 displayed in R, G, B. (For interpretation of the references to colour in this figure legend, the reader is referred to the web version of this article.)

October (White et al., 2002). Forest phenology was considered when choosing appropriate remote sensing image acquired in leaf-on season. Areal coverage of forest and non-forest classes is approximately equal in the VM study area.

Located in central Brazil, centered at 9°36′52.86″S, 50°12′34.69″W and covering 47.5-by-26.1 km area, the Mato Grosso-Tocantins-Pará (MTP) study area lies within the southeastern frontier of the Amazon rain forest and has experienced widespread forest loss due to agricultural expansion. The region's tree species diversity is exceptionally high and the predominant evergreen forest phenology is not a dominant factor when selecting satellite image dates. Instead, cloud cover is a stronger limitation on data quality. Before these forest losses took place, the MTP study area was mainly covered by forest with a very small proportion of other land cover classes.

2.2. Landsat data

Landsat images were collected from three epochs: mid-1980s, circa-1990, and circa-2000 (Table 1). For each site, the mid-1980s image was downloaded from the USGS. The latter two images were part of the Global Land Survey (GLS), a collection of images optimally selected for land cover change detection and orthorectified to within one pixel geolocation accuracy (Gutman et al., 2008; Tucker et al., 2004). A Landsat Multi-Spectral Scanner (MSS) image, representing a circa-1970 epoch, was also included for the VM study area but not for the MTP study area due to lack of high-quality MSS image.

2.3. Corona data

Corona images were originally photographed by panoramic cameras and recorded on film, with strong response in the visible spectrum (400–700 nm). The data were digitized to 8-bit radiometric precision with only one "panchromatic" band and are distributed by the USGS at nominal ground resolutions of 9 feet and 6 feet (~2.74 m and 1.83 m) (Galiatsatos, 2009). Each Corona scene has an approximate ground coverage of 17 by 232 km in the KH 4A mission and 13.8 by 188 km in the KH 4B mission (Galiatsatos, 2009). Corona images used in this study were mainly acquired in KH 4A and 4B missions in 1966 and 1967 (Table 2). Due to variations in pixel size and geometric distortions resulting from the wide view angles of the cameras, geometric correction of entire Corona images was very challenging. In order to achieve satisfactory geometric correction results, we divided each Corona image into eight subsets along the cross-track direction, and one subset from each of the two study areas was selected for analysis (see Table 2).

3. Methods

Images gathered by sensors aboard the Corona satellites have different spectral coverage (e.g. panchromatic vs. multispectral) and ground resolutions (e.g. ~2 m vs. 30 m) than images acquired by Landsat Thematic Mapper (TM) or Enhanced Thematic Mapper Plus (ETM+) sensors. Change detection methods based on directly measuring differences of spectral responses between dates (Coppin et al., 2004; Macleod and Congalton, 1998; Singh, 1989) cannot be applied to data of such different radiometric and spatial characteristics. Spatial and radiometric differences thus necessitated independent image preparation and a post-classification approach to change detection.

Corona images were used to derive forest classifications for the 1960s, and the Landsat images were analyzed using an automated change-mapping algorithm to map forest-cover change in later

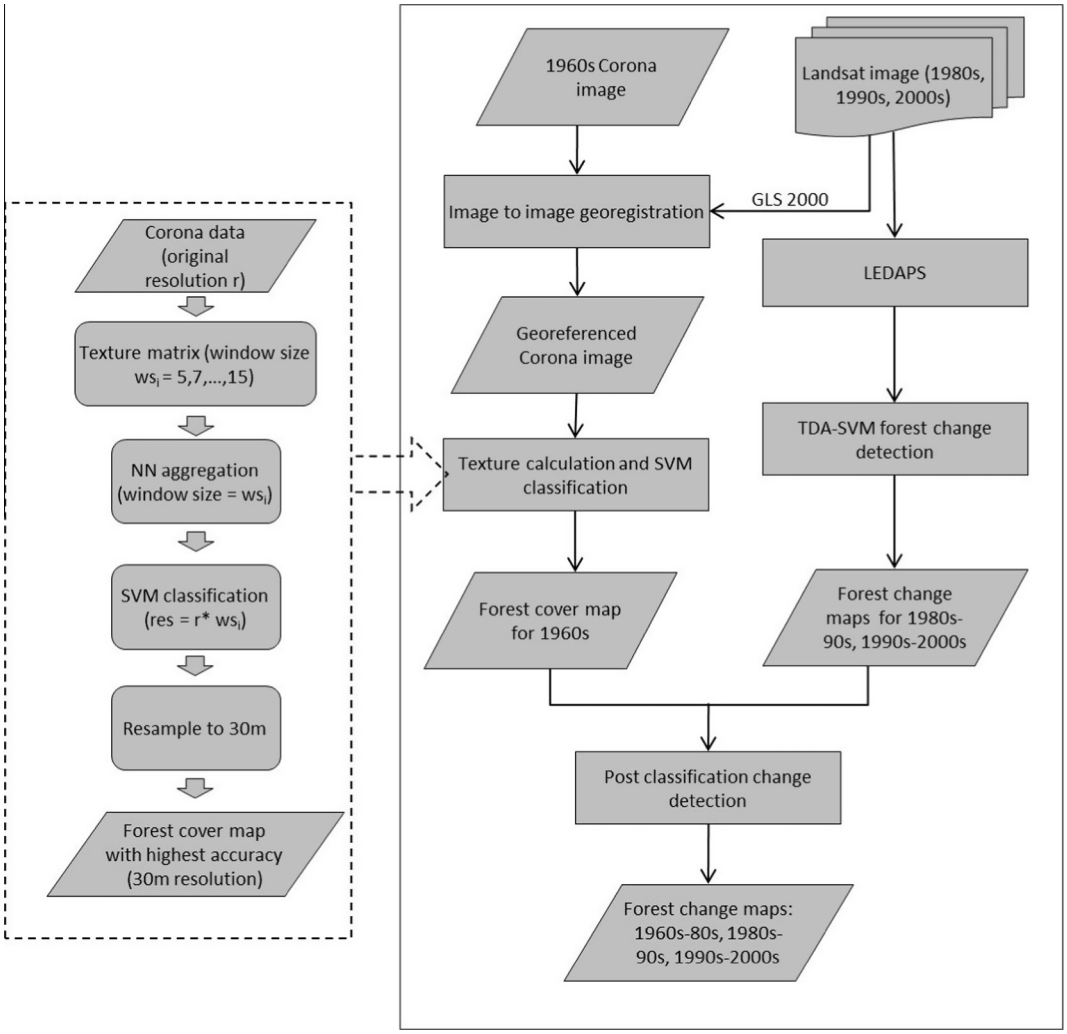

Fig. 3. Forest change mapping procedure. The flowchart in the solid frame is the overall procedure and the one in the dotted frames shows the steps of texture-based classification of Corona data.

Table 1
WRS-2 and WRS-1* path/row numbers, sensors and acquisition dates of Landsat images used in this study.

VM study area				MTP study area			
Path	Row	Acq. date	Sensor	Path	Row	Acq. date	Sensor
16*	33*	10/11/1972	MSS	–	–	–	–
15	33	09/15/1985	TM	223	67	07/17/1986	TM
15	33	05/16/1987	TM	223	67	07/25/1992	TM
15	33	10/05/2001	ETM+	223	67	09/01/2000	ETM+

Table 2
Properties of Corona images (Galiatsatos, 2009; NPIC 1967) used in this study.

	VM study area	MTP study area
Acquisition date	09/25/1967	06/22/1966
Spatial resolution	6 ft. (~1.83 m)	9 ft. (~2.74 m)
Camera	Forward looking	Afterward looking
Field of view	5° (along track)	5° (along track)
Scan angle	70° (+/− 35° from track)	70° (+/− 35° from track)

periods. The maps derived from Corona and Landsat data were then combined to quantify forest-cover changes across the consecutive epochs from the 1960s to 2000s (see Fig. 3). The Landsat methods have been described in previous publications (Feng et al., 2012a; Huang et al., 2008; Masek et al., 2006) and so are only outlined here. The remainder of this section focuses on methods for processing Corona images.

3.1. Landsat forest cover change mapping

Landsat TM and ETM+ images were atmospherically corrected to estimates of surface reflectance using the Landsat Ecosystem Disturbance Adaptive Processing System (LEDAPS) implementation of the 6S atmospheric correction algorithm (Feng et al., 2012a; Masek et al., 2006). Forest changes between consecutive epochs from 1980s to 2000s (e.g. 1980s–1990s) were then mapped using the Training Data Automation-Support Vector Machine (TDA-SVM) algorithm (Huang et al., 2008), which trains an SVM-based classification on a sample of "forest" pixels automatically identified using an a priori dark-vegetation heuristic rule. Clouds and their shadows were identified based on visible and thermal properties and masked from the dataset (Huang et al., 2010). Landsat MSS image was classified using SVM based on forest and non-forest training samples collected through visual interpretation. Post classification change detection method was applied to map forest cover change between 1970s and 1980s. Pixels identified as cloud or cloud-shadow in any epoch were excluded from further analysis.

Table 3
Texture measures used in this study and their sources.

References	Texture measurements
Haralick et al. (1973)	Angular second-moment (ASM), CON, COR, CO-VAR, inverse different moment, sum average, sum CO-VAR, sum CO-ENT, CO-ENT, difference variance, difference CO-ENT, information measure of COR, max COR.
Kushwaha et al. (1994)	ASM, ENT, inverse difference moment
Anys et al. (1994)	First order: MN, ENT, standard deviation, SKE; Second order: absolute value, CO-ENT, CON, COR, CO-VAR, cluster prominence; Third order: absolute value, OC-ENT, CON, small number emphasis, depth emphasis
Hudak and Wessman (1998)	Standard deviation
Shaban and Dikshit (2001)	GLCM, grey level difference histogram (GLDH), sum and difference histogram (SADH)
Clausi (2002)	CON, COR, C-ENT.
Kim et al. (2011)	ASM, CONT, COR, DIS, CO-ENT, HOM, MN, CO-VAR.
This study	Occurrence texture: DR, MN, OC-VAR, OC-ENT, SKE; Co-occurrence texture: CO-VAR, HOM, CON, DIS, CO-ENT, SM, COR. Texture combination 1(COMB1): HOM + CO-ENT + COR + MN Texture combination 2(COMB2): DIS + SM + CO-VAR + MN

3.2. Corona forest cover mapping

3.2.1. Geometric correction

Geolocation information distributed with Corona images includes only approximate coordinates of image corners, and preliminary inspection revealed that images selected in this study had spatial errors of several kilometers. Corona images were therefore registered to orthorectified GLS Landsat images. For each site, the Corona image was coregistered to the GLS 2000 image using road intersections and other stable ground features as ground control points (GCP). These GCPs (totaling 19 in the VM site and 8 in the MTP site) were manually selected through careful inspection of the Corona and Landsat images. In addition, 15 GCPs in the VM site and 10 GCPs in the MTP site were identified and used for independent assessment of registration accuracy. Several polynomial functions for coregistering the Corona images to Landsat data were tested, and the one with lowest RMSE was selected to correct the Corona image.

3.2.2. Texture analysis

Panchromatic Corona images have limited spectral information for forest cover classification. However, their high spatial resolution allows calculation of texture measures at various spatial resolutions. Many of these texture measures were found useful to visually discriminate different land cover types land cover discrimination (see Table 3 and Fig. 4).

To evaluate the utility of texture measures for separating forest and non-forest in Corona data, we evaluated both occurrence (first-order) and co-occurrence (second-order) texture measures. Five occurrence textures were selected due to their effectiveness in land cover classification (Anys et al., 1994). Seven relatively uncorrelated and widely used co-occurrence textures (Anys et al., 1994) out of fourteen statistical features proposed by Haralick et al. (1973) were also selected. Occurrence metrics tested included data range (DR), variance (OC-VAR), mean (MN), entropy (OC-ENT) and skewness (SKE):

$$DR = GL_{\max} - GL_{\min}$$

$$MN = \sum_{i=0}^{L-1} i * P(i)$$

$$OC - VAR = \sum_{i=0}^{L-1} (i - MN)^2$$

$$OC - ENT = -\sum_{i=0}^{L-1} P(i) * \log_2[P(i)]$$

$$SKE = \frac{1}{(OC - VAR)^{3/2}} * [\sum_{i=0}^{L-1} (i - MN)^3 * P(i)]$$

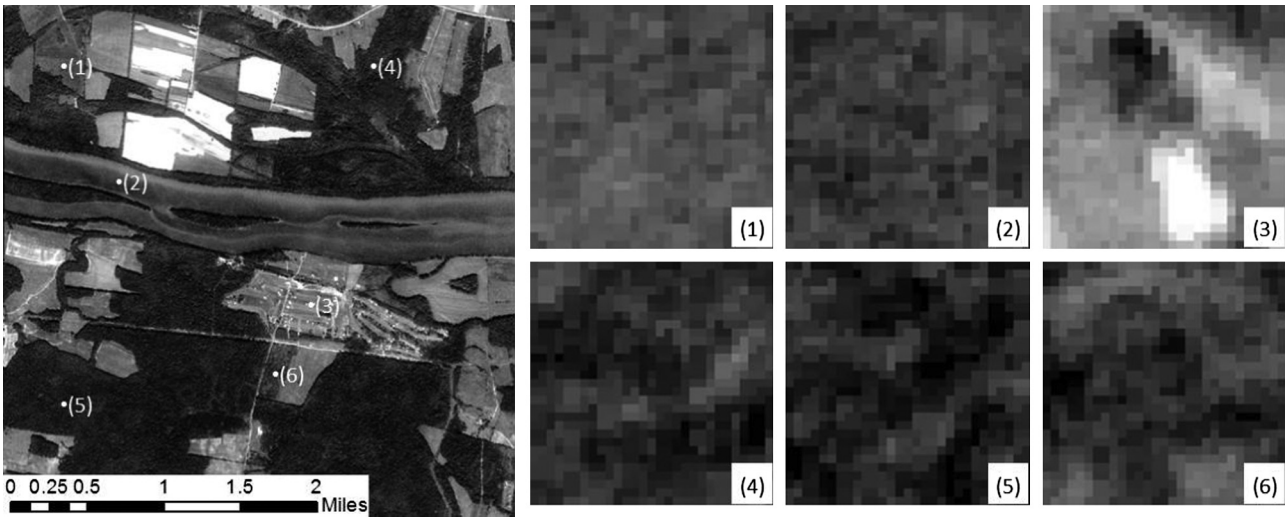

Fig. 4. Corona image, aggregated to 27.5 m resolution, in the left window has multiple land cover types, including forest, cropland, water body and scattered build-ups. Zoom-in windows 1, 2 and 3 show non-forest land cover, window 4 and 5 show dense forest cover and scatter forest cover is presented in window 6.

where L is the maximum grey level (GL), $P(i)$ is the frequency of pixels where GL = i in a window, and "max" and "min" are the maximum and minimum value within a window. Co-occurrence texture measures included variance (CO-VAR), homogeneity (HOM), contrast (CON), dissimilarity (DIS), entropy (CO-ENT), second moment (SM), and correlation (COR):

$$CO-VAR = \sigma_x + \sigma_y$$

$$CO-ENT = \sum_{i=0}^{L-1}\sum_{j=0}^{L-1} P(i,j,d,\theta) * \log_2(P(i,j,d,\theta))$$

$$CON = \sum_{i=0}^{L-1}\sum_{j=0}^{L-1} (i-j)^2 * P(i,j,d,\theta)$$

$$COR = \sum_{i=0}^{L-1}\sum_{j=0}^{L-1} [(i-\mu_x) * (j-\mu_y) * P(i,j,d,\theta)]/(\sigma_x * \sigma_y)$$

$$HOM = \sum_{i=0}^{L-1}\sum_{j=0}^{L-1} P(i,j,d,\theta)/(1+(i-j)^2)$$

$$DIS = \sum_{i=0}^{L-1}\sum_{j=0}^{L-1} (i-j) * P(i,j,d,\theta)$$

$$SM = \sum_{i=0}^{L-1}\sum_{j=0}^{L-1} P(i,j,d,\theta)$$

where $P(i,j,d,\theta)$ is the frequency of co-occurrence between pixels where GL = i and those where GL = j given distance between the two pixels is d and direction of displacement is the angle θ (Anys et al., 1994). σ_x and σ_y are the standard deviation of lines and columns of the Grey Level Co-occurrence Matrix (GLCM), and μ_x and μ_y are the means of lines and columns of the same matrix.

To evaluate the impact of window size on class separability, the texture measures were calculated using window sizes (n) of 5 × 5-pixel, 7 × 7-pixel, 9 × 9-pixel, 11 × 11-pixel, 13 × 13-pixel, and 15 × 15-pixel at the original resolution (r) of the Corona images. Each texture image was resampled using the same window size with the nearest neighbor (NN) resampling method to produce a texture image at spatial resolution of r^*n.

3.2.3. SVM classification of the Corona data

Reflectance and texture metrics were used to derive forest/non-forest classifications using Support Vector Machines (SVM) (Chan et al., 2001; Huang et al., 2002; Pal and Mather, 2005), an advanced machine learning algorithm designed to locate an optimal multivariate boundary between classes. Distributed across each study area, training data included 4641 forest and 4618 non-forest pixels in the VM study area and 2272 forest and 3580 non-forest pixels in the MTP study area (Table 4). The non-forest class comprised bare soil, herbaceous vegetation, water, and other cover features, and so a larger portion of non-forest pixels were sampled than their true proportion in the MTP study area in order to characterize the range of variability within this complex class. Training pixels were labeled through visual interpretation of the Corona images at their native resolution by an experienced image analyst. Because SVM requires training samples located near the discrimination boundary between two classes in the feature space (Huang et al., 2002), some mixed pixels were deliberately included in the training sample. Edge pixels were included to represent high texture values near edges. The radial basis function (RBF) kernel was used because it has been found to be robust for various classification problems (Huang et al., 2002). Optimal values for the cost parameter c and the RBF kernel parameter γ were selected through five-fold cross validation following the procedure in Chang and Lin (2011). We first varied the parameter values at coarse steps and, once the approximate ranges of the optimal parameter values were determined, finer steps were used to optimize parameter values within the approximate ranges.

To evaluate the utility of various texture measures for forest/non-forest classification, we ran the SVM with different combinations of texture measures together with the panchromatic brightness values (i.e., MN) (Table 5). For each set of texture inputs, the SVM parameters that yielded the highest cross-validation accuracy for a study area were chosen and used to classify the entire image subset for that area. Since our goal was to use these classifications together with results derived from Landsat to estimate forest change, all classifications derived using the Corona data were aggregated to 30-m resolution using a majority rule.

Table 4
Number of training and validating pixels used for forest and non-forest classification using Corona data in each study site.

Study site	Training pixels		Validating pixels	
	Forest	Non-forest	Forest	Non-forest
VM	4641	4618	1064	926
MTP	2272	3580	1313	184

3.3. Accuracy assessment of forest cover and change products

Forest cover and change classifications were evaluated using overall accuracy, kappa coefficient, and class-specific user's and producer's accuracies derived from a confusion matrix (Congalton, 1991; Stehman and Czaplewski, 1998). Reference data were collected by stratified random sampling with strata defined by land cover classes in the output forest cover and change maps (i.e. forest, non-forest, forest gain, and forest loss). This approach is commonly incorporated in sampling design for accuracy assessment of global to regional land cover maps (Olofsson et al., 2012). Stratified random sampling is a probability-based sampling method, which enhances the precision of accuracy estimates for minor classes. It is thus advantageous over simple random sampling in reducing the standard error for estimating overall accuracy (Stehman, 1999; Stehman and Czaplewski, 1998). For each selected

Table 5
Texture features used in the classifications, windows sizes to derive textures, scales at which classifications and corresponding accuracy assessments were carried out at the VM study area.

Texture features	Window size*	Classification resolution*	Accuracy assessment resolution
MN	5 × 5, 7 × 7, 9 × 9, 11 × 11, 13 × 13, 15 × 15-pixel	9.14 m, 12.80 m, 16.50 m, 20.12 m, 23.77 m, 27.43 m	30 m
DR + MN			
OC-ENT + MN			
SKE + MN			
OC-VAR + MN			
CON + MN			
COR + MN			
DIS + MN			
CO-ENT + MN			
HOM + MN			
SM + MN			
CO-VAR + MN			
ALL TEXTURES			
HOM + CO-ENT + COR + MN			
DIS + SM + CO-VAR + MN			

* *Note*: at MTP study area, window sizes are 5 × 5, 7 × 7, 9 × 9, 11 × 11, and classification resolution is 13.7 m, 19.04 m, 24.66 m and 30.14 m, other parameters are the same as the VM study site.

Table 6
Number of validation pixels for assessing Landsat-based FCC (1980s–2000s) products at each study area.

Study site	1970s FC		1980s–1990s FCC				1990s–2000s FCC			
	Forest	Non-forest	Persistent Forest	Forest loss	Forest gain	Persistent non-forest	Persistent forest	Forest loss	Forest gain	Persistent non-forest
VM	922	596	977	72	59	874	853	183	81	865
MTP	–	–	1436	67	6	433	1430	11	1	500

pixel, the true forest-change type was determined by visual comparison of the Landsat series against high-resolution images from Google Earth, similar to the method described by Feng et al. (2012b). A summary of the reference sample for evaluating the Landsat-based cover and change maps is provided in Table 6. Reference samples for evaluating the Corona classifications were also selected randomly within forest and non-forest stratum in both study areas. For the classification derived from Corona data, each sample pixel was labeled as forest or non-forest at 30-m resolution based on visual analysis of the Corona images at their native resolutions. The number of reference samples for each class in each study area is listed in Table 4.

3.4. Forest cover change rate calculating

The Corona-based, 30-m forest/non-forest classifications with highest accuracies were used together with the Landsat-based FCC products to calculate forest cover and change rates between the 1960s and 2000s for the two study areas. Gross forest loss and gain rate were converted to average annual change rate by dividing the rate of gross loss or gain to the total land area by the time difference (in years) of each pair of images.

$$\text{Average annual loss rate (\%)} = \text{total loss area/total land area/year difference} * 100$$

Table 7
RMSE of Corona image geometric correction at two study areas.

Study area		VM		MTP	
		Control points	Check points	Control points	Check points
Number of points		19	15	8	10
RMSE (meters)	x	8.08	15.29	11.38	20.33
	y	6.05	10.28	4.58	21.18
	Total	10.09	18.24	12.29	29.35

$$\text{Average annual gain rate (\%)} = \text{total gain area/total land area/year difference} * 100$$

4. Results

4.1. Geometric correction of Corona data

For both the VM and MTP sites, second-order polynomial transformations yielded the smallest root mean square errors (RMSE) for both the control and check GCPs. Corona images for both study areas were coregistered within one half pixel (15 m) of the Landsat data when measured using the control points (Table 7). Although the RMSE of check points were higher than those of control points, suggesting some model over-fitting. Control-point errors were still less than one 30-m pixel. The geolocation accuracy of corrected Corona image was comparable to the Landsat images themselves (Tucker et al., 2004), so few spurious change detection would be caused due to misregistration. The greater co-registration errors in the MTP site were likely due to lack of road intersections and other stable ground features that could be used as GCPs. As a result, river banks and some small water bodies were selected as GCPs, some of which could have moved during the period between the Corona and Landsat data acquisitions (see Table 7).

4.2. Effectiveness of textures for Corona forest/non-forest classification

Accuracies of the Corona-based forest/non-forest classifications derived using various combinations of texture measures calculated using different window sizes are shown in Fig. 5. The overall accuracies in the VM study area ranged from 90.5% to 95%, with Kappa coefficients between 0.81 and 0.90 (Fig. 5). The maximum overall accuracy and Kappa statistic were approximately 95% and 0.9, respectively. Except for the classification derived using mean reflectance (MN) alone, the overall accuracies and Kappa coefficients in the MTP ranged from 94.5% to 96.5% and from 0.75 to 0.82 respectively.

Table 8
Accuracies of TDA-SVM forest change map.

Accuracy measure	Persistent forest	Persistent non-forest	Forest loss	Forest gain
VM study area, WRS2 path 015/row 033				
1980s–1990s epoch, overall accuracy = 91.99%, kappa coefficient = 0.87				
User's accuracy (%)	95.00	93.08	88.89	76.19
Producer's accuracy (%)	88.37	96.1	82.76	88.89
1990s–2000s epoch, overall accuracy = 91.67%, kappa coefficient = 0.87				
User's accuracy (%)	98.36	96.53	74.51	84.38
Producer's accuracy (%)	80.00	97.20	97.44	90.00
MTP study area, WRS2 path 223/row 067				
1980s–1990s epoch, overall accuracy = 95.59%, kappa coefficient = 0.89				
User's accuracy (%)	97.30	95.92	87.50	62.50
Producer's accuracy (%)	99.08	90.38	73.68	83.33
1990s–2000s epoch, overall accuracy = 86.51%, kappa coefficient = 0.80				
User's accuracy (%)	98.00	95.00	70.00	50.00
Producer's accuracy (%)	90.74	80.85	82.35	100.00

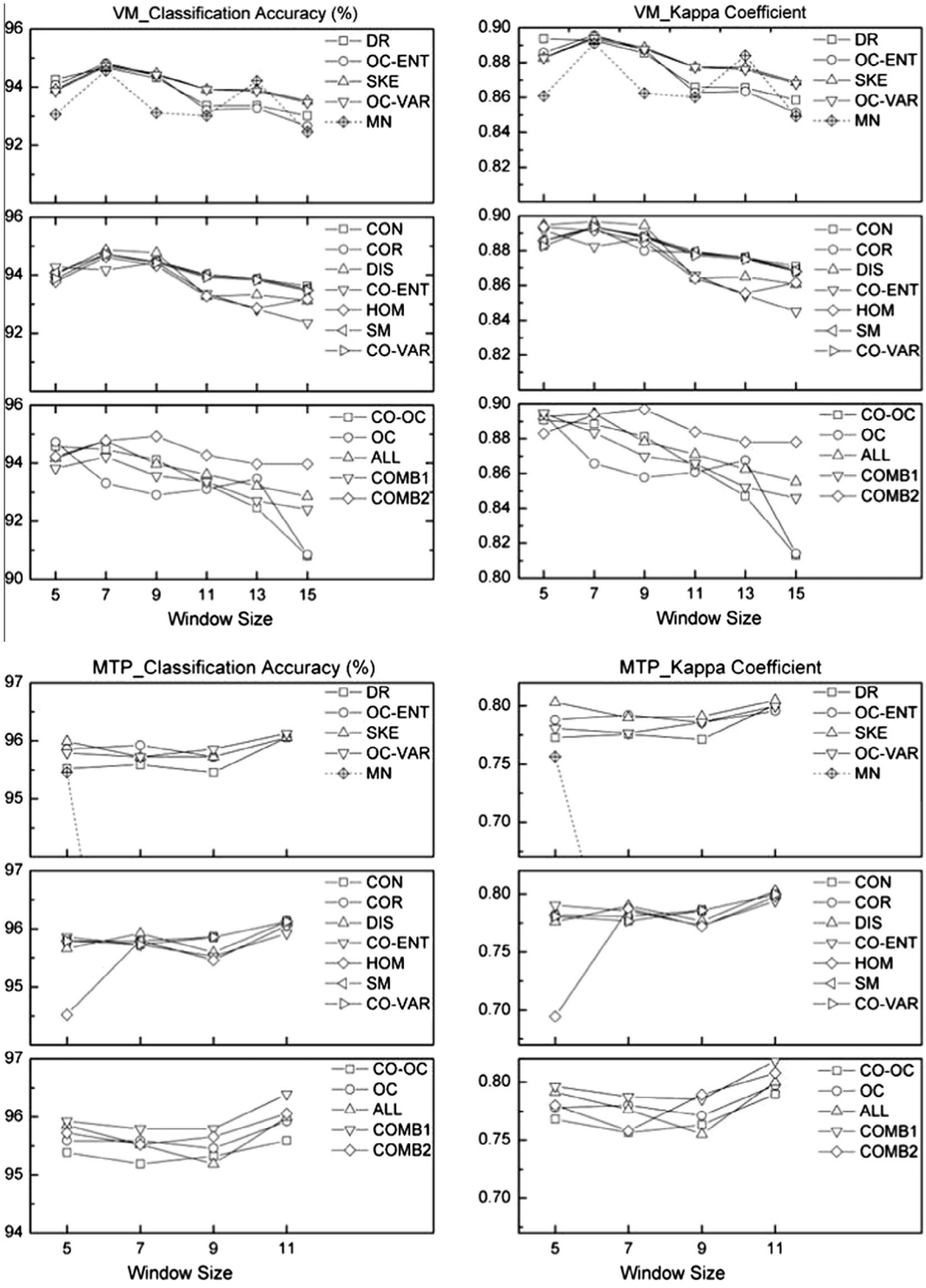

Fig. 5. Classification accuracies and kappa coefficients of Corona forest/non-forest classifications using single and multiple textures in the VM and MTP study areas. Abbreviations are defined in Table 3. For the MTP study area, the value of classification using MN fell below the range of *y*-axis, kappa coefficients were 0.52, 0.57 and 0.46 at window sizes of 7×7 to 11×11, and classification accuracies were 88.0%, 89.6% and 85.1% correspondingly.

Some of the texture measures may not be suitable for forest/non-forest classification using Corona data. In the MTP site, accuracies derived using MN alone within window sizes > 5 pixels were substantially lower than those derived using texture measures. MN also yielded lower accuracies when calculated using window sizes of 5×5 and 9×9 pixels. In the VM site, occurrence (OC) and co-occurrence (CO-OC) textures calculated using a window size of 15 pixels also yielded markedly lower accuracies. Accuracies derived using the other texture measures differed by up to 4% (or 0.04), but no individual texture measure had consistently better accuracies than the others. Interestingly, and likely due to model over-fitting, use of all texture measures (ALL) did not yield the best accuracies. However, in the VM site, the combination of HOM, CO-ENT, COR and MEAN (COMB2) calculated using window sizes of 9 pixels or larger seemed to have slightly better accuracies than all other texture combinations, while in the MTP site, the combination of DIS, SM, CO-VAR, and MEAN (COMB1) had marginally better accuracies.

Performances of different textures calculated at the same window size usually do not vary much but the impact of varying window size on accuracies had obvious patterns (Fig. 5). In the VM site, windows of 7 × 7 to 9 × 9 pixels (or ~13 × 13 m to ~16 × 16 m) yielded best accuracies for most texture measures, but accuracy decreased with window size. In the MTP site, the window size of 11 × 11 pixels (or ~30 m × 30 m) yielded the best accuracies for most texture measures. Although land cover in the VM study area shows more heterogeneous pattern than that in the MTP site, patch size of forest land in eastern U.S. is much smaller than that in the undeveloped Amazon rainforest. In the VM site, small forest patches result in more mixed pixels, which can be better captured by textures calculated from relatively small window sizes. Overestimation of forest was caused as window size increased to 15 × 15 pixels. On the other hand, peppered non-forest pixels were mapped as random speckle in homogeneous forests in the MTP site when small window sizes were used. The use of windows as large as 11 × 11 pixels avoided the misclassification of non-forested pixels caused by poor image quality in this site.

4.3. Accuracy of Landsat forest cover change map

Overall accuracies were > 91% for both the 1980s–1990s and 1990s–2000s periods in the VM study area, and were 96% and 87% for the two periods in the MTP area (see Table 8). Both persistent forest and persistent non-forest had user's accuracies > 90% in all periods and producer's accuracies > 90% in the majority of periods. The forest-loss class had slightly lower accuracies, but its user's and producer's accuracies were > 70% in both sites during both periods. The forest-gain class had lower user's accuracies in

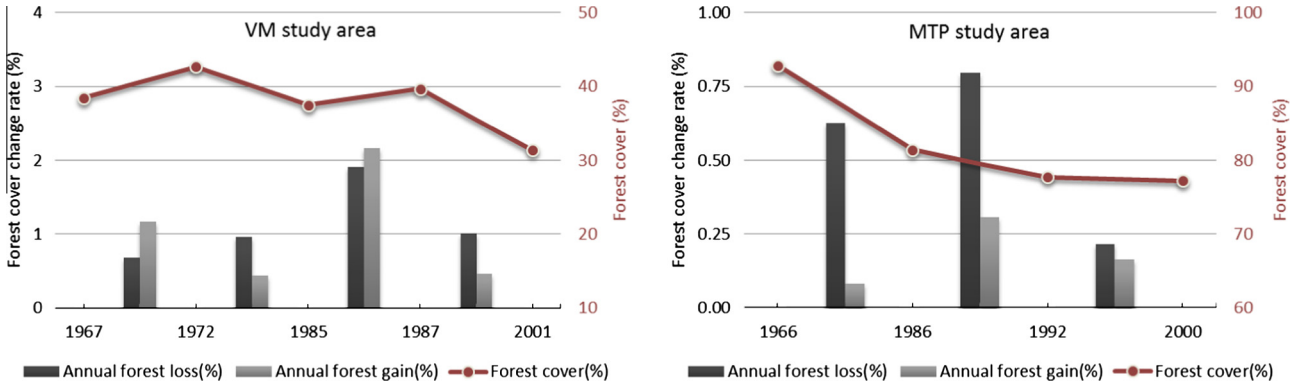

Fig. 6. Forest cover change rates during three epochs for two study areas, forest loss (or gain) percentage = forest loss (or gain) area/forest area of beginning year * 100.

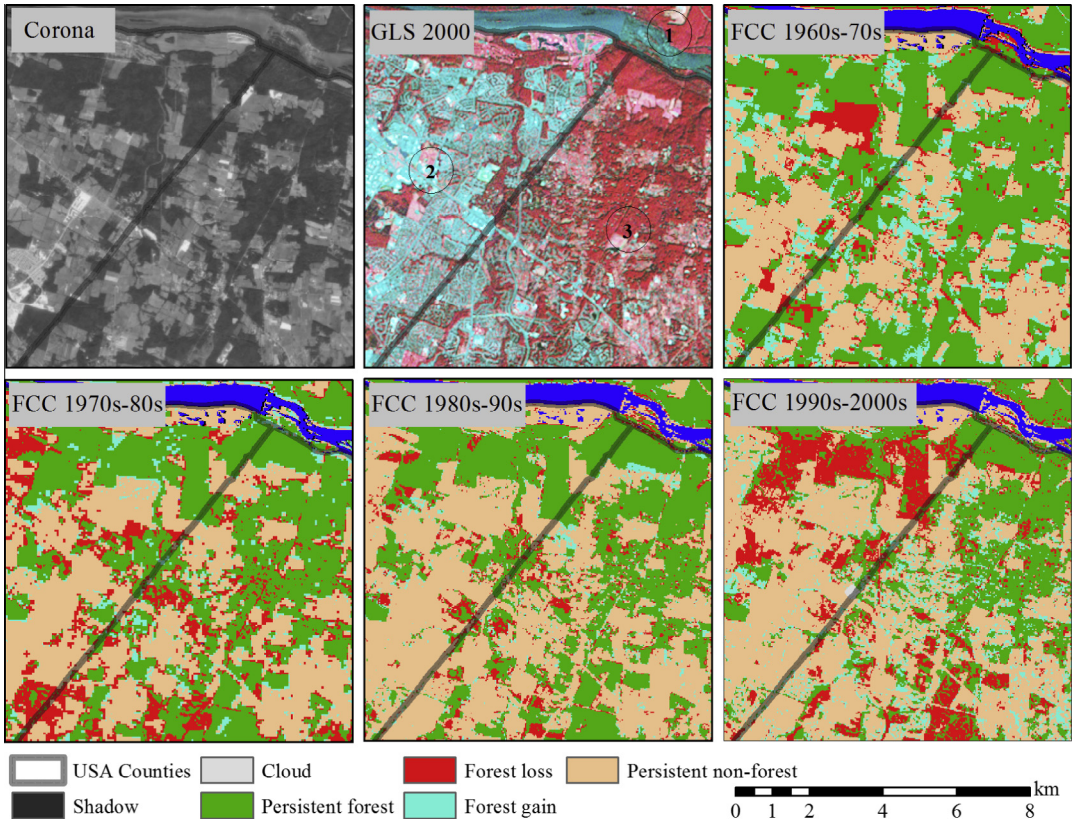

Fig. 7. Georeferenced Corona, GLS 2000 images with band 4, 3, 2 in color R, G, B, and sequential forest cover change maps of each two epochs in the VM study area. (1) is Montgomery County in Maryland, (2) and (3) is Loudoun and Fairfax County in Virginia separately. (For interpretation of the references to colour in this figure legend, the reader is referred to the web version of this article.)

the MTP site (62.5% and 50%), likely because the coverage of forest gains was very low, so only a small number of reference points were randomly sampled for estimating the accuracy for this class. Commission error increased significantly when the forest class was overestimated in time two; this led to reduced user's accuracy especially in forest gains. Overall accuracy of GLS1975 image classification achieved 94% with overall kappa coefficient of 0.89.

4.4. Forest cover change rate

The highest-accuracy of the 30-m resolution map of forest cover based on Corona images was obtained by using the second texture combination (COMB2), calculated with window size of 9 for the VM study area and using the first texture combination (COMB1), calculated with window size of 11 for the MTP study area. Although both study areas lost substantial forest cover between the 1960s and 2000s, they had different forest change histories (Fig. 6). Located in the suburbs of Washington, DC and the Chesapeake Bay region, the VM study area comprised areas in Fairfax and Loudoun Counties, Virginia and Montgomery County, Maryland (Fig. 7). The annual forest loss rate during mid-1980s doubled to 2%. Most of the loss happened before the 1980s and after the 1990s, especially in Loudoun County in Virginia. Annual forest gain rates were ~1% during the 1960s and the 1970s, then increased to ~2%–exceeding forest loss rate during the 1980s—and dropped afterwards. Most trees appear to have been planted around residential areas. As a result, forest cover in the VM study area slightly increased around late 1980s and then continued decreasing.

In contrast, the rate of annual forest loss in the MTP study area was relatively low (~0.6–0.76%) from the 1960s to the 1990s and dropped to ~0.2% during the period of 1992–2000. However, the patch size of cleared forest was much larger than in the VM study area (Fig. 8), which was mainly cleared for cattle ranching and mechanized agriculture. The rate of forest gain was quite low (~0.1–0.26%) and was largely due to trees growing in abandoned agricultural land. Decrease of forest cover in the MTP study area continued from the 1960s to the early 1990s, driven by logging activities and gradually ceased till 2000.

5. Discussion

5.1. Value of Corona data for land cover change studies

The Landsat data record has been the primary sources for monitoring land cover change (Townshend et al., 2012). This record, however, only extends back to 1972. Many regions experienced forest loss prior to the Landsat era and many of these changes can be mapped through the combined use of CORONA and Landsat images. We have demonstrated images collected by the Corona instruments can be used together with those from Landsat to study land cover changes that have occurred since the 1960s. We have also shown that reforestation/afforestation occurred in two areas since the 1960s: in a suburban landscape in the temperate zone as well as an agricultural-wildland landscape in the tropics. In most eastern US, the 1960s represent the transition from forest regeneration due to agricultural abandonment to a period of forest logging and clearing (Drummond and Loveland, 2010). Annual carbon sequestration of forest has decreased since the late 1960s due to the acceleration of forest logging and clearing rates. Meanwhile, the carbon emission associated with the harvest of industrial wood was the region's largest source of carbon to the atmosphere (Houghton and Hackler, 2000). Tropical forest in South America remained intact till 1960s followed by severe loss, for instance, deforestation in Brazil's Amazon forest began with the construction of the Transamazon highway in 1970 (Fearnside, 2005). The annual release of carbon has increased over the period of 1850–1985 in South America, and half of the total occurred after 1960 (Houghton et al., 1991a). However, the most uncertain component in estimating carbon emission is related to historical rates of forest degradation and shifting cultivation, as well as the prior ecosystem type converted to human use (Houghton et al., 1991b).

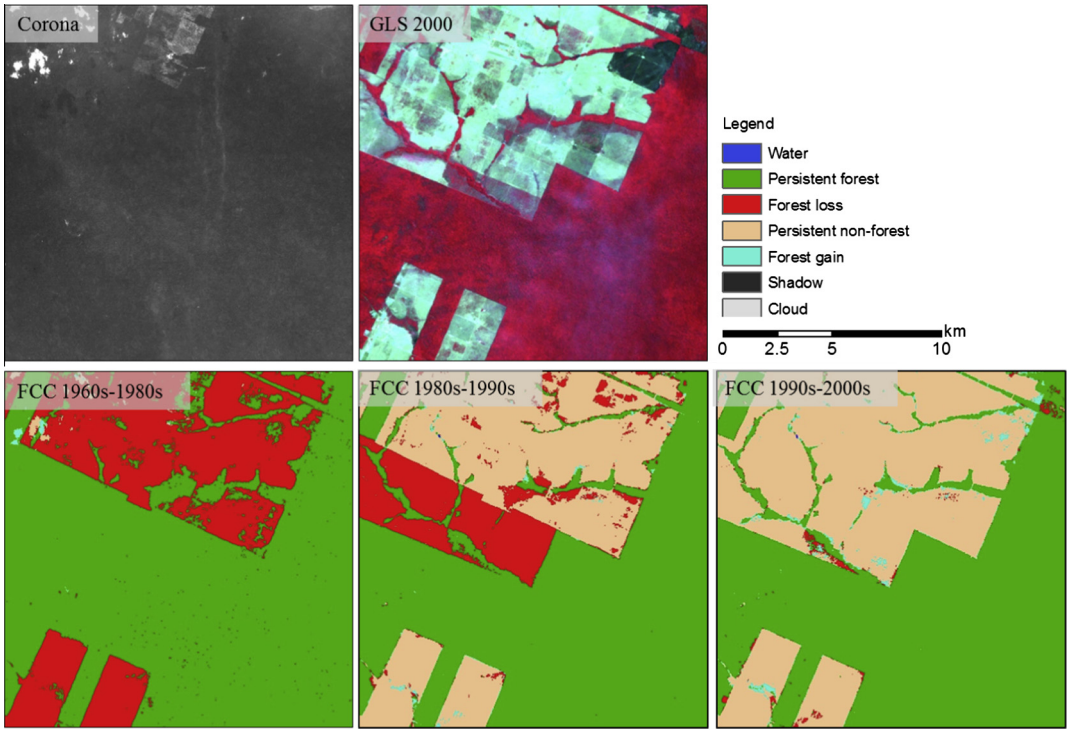

Fig. 8. Georeferenced Corona, GLS 2000 images with band 4, 3, 2 in color R, G, B, and sequential forest cover change maps of each two epochs in MTP study area. (For interpretation of the references to colour in this figure legend, the reader is referred to the web version of this article.)

With high spatial resolutions of 1.83–2.74 m (6–9 feet), which are comparable to or even better than the resolutions of recently launched, high-resolution commercial satellites, Corona data allow for reliable identification of forest and other land cover types. Although Corona images were recorded on film with limited spectral information, their high spatial resolution greatly improves interpretability through visual analysis. This also allows accurate mapping and validation when reference data is absent for 1960s for many areas. Moreover, Corona images provide a unique documentation of the 1960s for most areas of the globe (Fig. 1), which especially benefits regions that do not have early air-borne images. The affordable price (30 USD per scene) can further leverage the wide use of this dataset. All these facts indicate that Corona data can be widely used in studying the forest cover or land cover land use changes in 1960s and can greatly reduce the uncertainties in estimating carbon emission from 1960s.

5.2. Need for automation in large-area applications

In this study, Corona images were used with Landsat images to monitor forest cover and its changes in a suburban study area and a tropical forest area. Co-registration against terrain-corrected Landsat images yielded high georegistration accuracy of Corona images using manually selected GCPs and polynomial transformation functions. The co-registered Corona images were deemed to have adequate geolocation accuracy for comparison against Landsat images for mapping forest change without introducing excessive spurious changes (Townshend et al., 1992). However, more rapid or automated georeferencing methods, such as the Automated Registration and Orthorectification Package (AROP) (Gao et al., 2009), will be required to deal with large volumes of images necessary for studying larger regions. Any such method must be capable of overcoming spectral and resolution differences between Corona and Landsat, as well as real differences in land cover accumulated over long times.

The classification method we developed here has improved in processing efficiency compared to visual interpretation and/or manual delineation of land cover used in previous studies (Bindschadler and Vornberger, 1998; Challis et al., 2002). The use of texture measures increased the accuracy of classification compared to only using image grey-scale values alone. The combination of co-occurrence textures representing different spatial patterns with grey-scale value is recommended for studies in the future. While, different forest classes can hardly be separated so far using only texture information. Additionally, although the best window size for extraction of textural measurements is usually affected by image spatial resolution, vegetation structure, and forest patch sizes in landscape (Lu et al., 2008), small window sizes (e.g., 9×9 pixels) are recommended for both complex and homogeneous landscapes. Beyond the texture measurements we used for separating forest and non-forest class, automatic tree crown identification algorithm proposed by Palace et al. (2008) could potentially be applied to Corona image, given its very high spatial resolution and panoramic, to estimate tree crown width and percent tree cover in 1960s. Given the availability of adequate, representative training data, effective classification features and improvements in automated image registration, forest classification and change detection using Corona image can be automated for large areas around the globe.

6. Conclusions

The Landsat satellites have generated a primary source of information for studying changes in Earth's land surface that now spans four decades since the 1970s. Using data acquired from Corona satellites, which have spatial resolutions better than Landsat data and are available for most of the land areas of the globe, this record can be extended a decade further, to the 1960s. We demonstrated the feasibility of paring Corona with Landsat images for mapping forest cover changes between the 1960s and 2000s through case studies conducted in two areas, Virginia-Maryland (VM) in the US and Mato Grosso-Tocantins-Pará (MTP) in Brazil. For each area, the Corona image was accurately co-registered to an orthorectified Landsat image. Combination of metrics to represent multiple aspects of spatial texture achieved classification accuracies of ~95%. Forest changes during the Landsat era were mapped with overall accuracies around 90%. Different forest-cover change rates and trends were observed between the two study areas, with 18.9% and 16.8% net forest loss in the VM and MTP study area respectively from 1960s to 2000s. Results based on Corona data indicate that forest area in a suburban study area of Virginia and Maryland increased from the 1960s to the 1970s, before being converted to residential area. In contrast, severe forest loss in the Amazon region started from scattered small forest land cleared during 1960s and 1970s and eventually expanded thereafter.

These results demonstrate the potential of Corona data in land cover and change studies. However, using Corona imagery for land cover change studies over larger areas will require more automated georegistration and classification methods. Georeferencing Corona images must be automated to avoid overwhelming human involvement, especially in the identification of ground control points. Automatic training data selection methods, similar to others used for Landsat-based classification, also need to be further developed for regional to global retrievals.

Acknowledgements

This work was performed at the Global Land Cover Facility (http://www.landcover.org/) with funding support from NASA's MEASURES (NNX08AP33A) program. Additional support was provided by NASA's Land Cover and Land Use Change Program. The publically available LIB-SVM code library (http://www.csie.ntu.edu.tw/~cjlin/libsvm/) (Chang and Lin, 2011) was used for classifying Corona and Landsat images. We would like to thank our colleagues Dr. Feng Gao at USDA-ARS Hydrology and Remote Sensing Laboratory, Dr. Kuan Song in University of Maryland Department of Geographical Sciences and Katie Collins at GLCF for providing technical support and improving the manuscript. We would also like to thank the anonymous reviewers for the comments.

References

Anys, H., Bannari, A., He, D.C., Morin, D., 1994. Texture analysis for the mapping of urban areas using airborne MEIS-II images.

Beck, A., Philip, G., Abdulkarim, M., Donoghue, D., 2007. Evaluation of Corona and Ikonos high resolution satellite imagery for archaeological prospection in western Syria. Antiquity 81, 161–175.

Bindschadler, R., Vornberger, P., 1998. Changes in the West Antarctic ice sheet since 1963 from declassified satellite photography. Science 279, 689–692.

Brandt, J.S., Kuemmerle, T., Li, H., Ren, G., Zhu, J., Radeloff, V.C., 2012. Using Landsat imagery to map forest change in southwest China in response to the national logging ban and ecotourism development. Rem. Sens. Environ. 121.

Casana, J., Cothren, J., 2008. Stereo analysis, DEM extraction and orthorectification of CORONA satellite imagery: archaeological applications from the Near East. Antiquity 82, 732–749.

Challis, K., Priestnall, G., Gardner, A., Henderson, J., O'Hara, S., 2002. Corona remotely-sensed imagery in dryland archaeology: the Islamic City of al-Raqqa, Syria. J. Field Archaeol. 29, 139–153.

Chan, J.C.-W., Huang, C., DeFries, R.S., 2001. Enhanced algorithm performance for land cover classification using bagging and boosting. IEEE Trans. Geosci. Rem. Sens. 39, 693–695.

Chang, C.-C., Lin, C.-J., 2011. LIBSVM: a library for support vector machines. ACM Trans. Intell. Syst. Technol. 2, 1–27.

Clausi, D.A., 2002. An analysis of co-occurrence texture statistics as a function of grey level quantization. Can. J. Rem. Sens. 28, 45–62.
Congalton, R., 1991. A review of assessing the accuracy of classifications of remotely sensed data. Rem. Sens. Environ. 37, 35–46.
Coppin, P., Jonckheere, I., Nackaerts, K., Muys, B., Lambin, E., 2004. Digital change detection methods in ecosystem monitoring: a review. Int. J. Rem. Sens. 25, 1565–1596.
Drummond, M.A., Loveland, T.R., 2010. Land-use pressure and a transition to forest-cover loss in the Eastern United States. Bioscience 60, 286–298.
Fearnside, P.M., 2005. Deforestation in Brazilian Amazonia: history, rates, and consequences. Conserv. Biol. 19, 680–688.
Feng, M., Huang, C., Channan, S., Vermote, E.F., Masek, J.G., Townshend, J.R., 2012a. Quality assessment of Landsat surface reflectance products using MODIS data. Comput. Geosci. 38, 9–22.
Feng, M., Huang, C., Sexton, J.O., Channan, S., Narasimhan, R., Townshend, J.R., 2012b. An approach for quickly labeling land cover types for multiple epochs at globally selected locations. In: Geoscience and Remote Sensing Symposium (IGARSS), 2012 IEEE International, pp. 6203–6206.
Galiatsatos, N., 2009. The shift from film to digital product: focus on CORONA imagery. Photogram. – Fernerkundung – Geoinform., 251–260.
Gao, F., Masek, J.G., Wolfe, R.E., 2009. Automated registration and orthorectification package for Landsat and Landsat-like data processing. J. Appl. Rem. Sens. 3.
Gutman, G., Byrnes, R., Masek, J., Covington, S., Justice, C., Franks, S., Headley, R., 2008. Towards monitoring land-cover and land-use changes at a global scale: the global land survey 2005. Photogram. Eng. Rem. Sens. 74, 6–10.
Haralick, R.M., Shanmuga, K., Dinstein, I., 1973. TEXTURAL FEATURES FOR IMAGE CLASSIFICATION. IEEE Transactions on Systems Man and Cybernetics, SMC3, pp. 610–621.
Houghton, R.A., Hackler, J.L., 2000. Changes in terrestrial carbon storage in the United States. 1: the roles of agriculture and forestry. Glob. Ecol. Biogeogr. 9, 125–144.
Houghton, R.A., Lefkowitz, D.S., Skole, D.L., 1991a. Changes in the landscape of Latin America between 1850 and 1985 I. Progressive loss of forests. For. Ecol. Manage. 38, 143–172.
Houghton, R.A., Skole, D.L., Lefkowitz, D.S., 1991b. Changes in the landscape of Latin America between 1850 and 1985 II. Net release of CO_2 to the atmosphere. For. Ecol. Manage. 38, 173–199.
Huang, C., Davis, L.S., Townshend, J.R.G., 2002. An assessment of support vector machines for land cover classification. Int. J. Rem. Sens. 23, 725–749.
Huang, C.Q., Song, K., Kim, S., Townshend, J.R.G., Davis, P., Masek, J.G., Goward, S.N., 2008. Use of a dark object concept and support vector machines to automate forest cover change analysis. Rem. Sens. Environ. 112, 970–985.
Huang, C.Q., Kim, S., Song, K., Townshend, J.R.G., Davis, P., Altstatt, A., Rodas, O., Yanosky, A., Clay, R., Tucker, C.J., Musinsky, J., 2009. Assessment of Paraguay's forest cover change using Landsat observations. Glob. Planet. Change 67, 1–12.
Huang, C., Thomas, N., Goward, S.N., Masek, J.G., Zhu, Z., Townshend, J.R.G., Vogelmann, J.E., 2010. Automated masking of cloud and cloud shadow for forest change analysis using Landsat images. Int. J. Rem. Sens. 31, 5449–5464.
Hudak, A.T., Wessman, C.A., 1998. Textural analysis of historical aerial photography to characterize woody plant encroachment in South African savanna. Rem. Sen. Environ. 66, 317–330.
Isaev, A.S., Korovin, G.N., Bartalev, S.A., Ershov, D.V., Janetos, A., Kasischke, E.S., Shugart, H.H., French, N.H.F., Orlick, B.E., Murphy, T.L., 2002. Using remote sensing to assess Russian forest fire carbon emissions. Clim. Change 55, 235–249.
Kadmon, R., Harari-Kremer, R., 1999. Studying long-term vegetation dynamics using digital processing of historical aerial photographs. Rem. Sens. Environ. 68, 164–176.
Kim, M., Warner, T.A., Madden, M., Atkinson, D.S., 2011. Multi-scale GEOBIA with very high spatial resolution digital aerial imagery: scale, texture and image objects. Int. J. Rem. Sens. 32, 2825–2850.
Kushwaha, S.P.S., Kuntz, S., Oesten, G., 1994. Applications of image texture in forest classification. Int. J. Rem. Sens. 15, 2273–2284.
Lu, D., Batistella, M., Moran, E., de Miranda, E.E., 2008. A comparative study of landsat TM and SPOT HRG images for vegetation classification in the Brazilian amazon. Photogram. Eng. Rem. Sens. 74, 311–321.
Macleod, R.D., Congalton, R.G., 1998. Quantitative comparison of change-detection algorithms for monitoring eelgrass from remotely sensed data. Photogram. Eng. Rem. Sens. 64, 207–216.
Masek, J.G., Vermote, E.F., Saleous, N.E., Wolfe, R., Hall, F.G., Huemmrich, K.F., Gao, F., Kutler, J., Lim, T.K., 2006. A Landsat surface reflectance dataset for North America, 1990–2000. IEEE Geosci. Rem. Sens. Lett. 3, 68–72.
McDonald, R.A., 1995. CORONA – success for space reconnaissance, a look into the cold-war, and a revolution for intelligence. Photogram. Eng. Rem. Sens. 61, 689–720.
Nagel, B.Y., 1991. Socioeconomic differentiation among small cultivators on Paraguay's eastern frontier. Latin Am. Res. Rev. 26, 103–132.
Nickson, A., 1981. Brazilian colonization of the Eastern Border Region of Paraguay. J. Latin Am. Stud. 13, 111–131.
NPIC, 1967. The KH-4A Camera System. In: National Photographic Interpretation Center.
Olofsson, P., Stehman, S.V., Woodcock, C.E., Sulla-Menashe, D., Sibley, A.M., Newell, J.D., Friedl, M.A., Herold, M., 2012. A global land-cover validation data set, part I: fundamental design principles. Int. J. Rem. Sens. 33, 5768–5788.
Pal, M., Mather, P.M., 2005. Support vector machines for classification in remote sensing. Int. J. Rem. Sens. 26, 1007–1011.
Palace, M., Keller, M., Asner, G.P., Hagen, S., Braswell, B., 2008. Amazon forest structure from IKONOS satellite data and the automated characterization of forest canopy properties. Biotropica 40, 141–150.
Richards, P.D., 2011. Soy, cotton, and the final Atlantic forest frontier. Prof. Geogr. 63, 343–363.
Rigina, O., 2003. Detection of boreal forest decline with high-resolution panchromatic satellite imagery. Int. J. Rem. Sens. 24, 1895–1912.
Sexton, J.O., Song, X.-P., Huang, C., Channan, S., Baker, M.E., Townshend, J.R., 2013. Urban growth of the Washington, D.C.–Baltimore, MD metropolitan region from 1984 to 2010 by annual, Landsat-based estimates of impervious cover. Rem. Sens. Environ. 129, 42–53.
Shaban, M.A., Dikshit, O., 2001. Improvement of classification in urban areas by the use of textural features: the case study of Lucknow city, Uttar Pradesh. Int. J. Rem. Sens. 22, 565–593.
Singh, A., 1989. Digital change detection techniques using remotely-sensed data. Int. J. Rem. Sens. 10, 989–1003.
Stehman, S.V., 1999. Basic probability sampling designs for thematic map accuracy assessment. Int. J. Rem. Sens. 20, 2423–2441.
Stehman, S.V., Czaplewski, R.L., 1998. Design and analysis for thematic map accuracy assessment: fundamental principles. Rem. Sens. Environ. 64, 331–344.
Tappan, G.G., Hadj, A., Wood, E.C., Lietzow, R.W., 2000. Use of Argon, Corona, and Landsat imagery to assess 30 years of land resource changes in west-central Senegal. Photogram. Eng. Rem. Sens. 66, 727–735.
Townshend, J.R.G., Justice, C.O., Gurney, C., McManus, J., 1992. The impact of misregistration on change detection. IEEE Trans. Geosci. Rem. Sens. 30, 1054–1060.
Townshend, J.R., Masek, J.G., Huang, C., Vermote, E.F., Gao, F., Channan, S., Sexton, J.O., Feng, M., Narasimhan, R., Kim, D., Song, K., Song, D., Song, X.-P., Noojipady, P., Tan, B., Hansen, M.C., Li, M., Wolfe, R.E., 2012. Global characterization and monitoring of forest cover using Landsat data: opportunities and challenges. Int. J. Digit. Earth, 1–25.
Tucker, C.J., Grant, D.M., Dykstra, J.D., 2004. NASA's global orthorectified Landsat data set. Photogram. Eng. Rem. Sens. 70, 313–322.
White, M.A., Nemani, R.R., Thornton, P.E., Running, S.W., 2002. Satellite evidence of phenological differences between urbanized and rural areas of the eastern United States deciduous broadleaf forest. Ecosystems 5, 260–273.